Surface Trapping of Atoms and Molecules with Dipole Rings

Hugo Dil,[1,2] Jorge Lobo-Checa,[1,2]* Robert Laskowski,[3] Peter Blaha,[3] Simon Berner,[1] Jürg Osterwalder,[1] Thomas Greber[1]†

The trapping of single molecules on surfaces without the formation of strong covalent bonds is a prerequisite for molecular recognition and the exploitation of molecular function. On nanopatterned surfaces, molecules may be selectively trapped and addressed. In a boron nitride nanomesh formed on Rh(111), the pattern consisted of holes 2 nanometers in diameter on a hexagonal superlattice, separated by about 3 nanometers. The trapping was further investigated with density functional theory and the photoemission of adsorbed xenon, where the holes were identified as regions of low work function. The analysis showed that the trapping potential was localized at the rims of the holes.

Although molecules can be trapped at surfaces by the formation of strong chemisorption bonds, for many applications as well for fundamental studies it is useful to trap molecules at specific parts of a surface through weak interactions that minimally perturb the bonding within the molecule. Surface dipoles, which contribute strongly to the bonding of polarizable entities, should be able to laterally immobilize molecules if they also exhibit in-plane components.

Electrostatic trapping caused by polarization-induced bonding offers a promising way to immobilize a molecule with minimal coupling to its support and neighbors. For atomic steps and kinks on surfaces, it is known that the lateral variation of the surface potential leads to strong electric fields parallel to the surface that may trap molecules (*1*, *2*). There are also recent reports on the immobilization and trapping of molecules with a chlorine center on defects of potassium bromide supports (*3*). Often, however, it is desirable to build structures that do not rely on random defects. Dislocation networks are periodic arrays of defects (*4*) on which molecules may be trapped. In this regard, hexagonal boron nitride (h-BN) nanomesh, a robust superstructure with a 3.2-nm lattice constant (*5*), has emerged as a promising basis for building nanostructures because it creates a ring of in-plane dipoles. For example, if naphthalocyanine, a molecule with a diameter of about 2 nm, is evaporated on the nanomesh, isolated molecular entities separated by 3.2 nm are found immobilized at room temperature (*6*). Nevertheless, not much is known about the nature of the trapping. Here, we propose a polarization-induced trapping mechanism on the basis of the observation of Xe conglomerates on the nanomesh.

It is now established that h-BN nanomesh on Rh(111) or Ru(0001) is a single sheet of h-BN, where 13 × 13 BN units form a coincidence lattice with 12 × 12 substrate unit cells (*6*–*8*). Two distinct BN regions were found: A closely bound region assigned to the "holes" or "pores" in the nanomesh and a loosely bound region assigned to the "wires" (*5*, *8*). Site-selective bonding of the BN nitrogen units to the substrate atoms creates a corrugation with an amplitude of about 0.05 nm and strongly affects the electronic structure (*8*). Theory confirmed the experimentally observed electronic structure (*5*–*7*) and showed the sp^2-derived σ-band density of states of the holes and the wires to be quasi-rigidly shifted with respect to each other by about 1 eV (*8*).

This finding suggests that a substantial portion of the h-BN σ-band shift is related to electrostatics; that is, to different work functions of the wires and the holes. The accompanying local vacuum-level misalignment imposes electric fields and leads to lateral polarization within the h-BN sheet. Heuristically, this structure may be described with dipole rings, which in turn offer a natural explanation for an enhanced immobilization of molecules. Permanent or induced dipoles in molecules are expected to have an affinity for the largest electrostatic potential gradients. The concept of in-plane dipoles at surfaces is reminiscent of the Smoluchowski effect on metallic surfaces, where delocalized valence electrons on steps or kinks cause the polarization (*9*). In the present case, the dipoles are formed by the contact of two regions with different work functions.

At room temperature, phthalocyanines (Pc's) diffuse on most flat surfaces and form islands (*10*, *11*). Instead, on the h-BN nanomesh, the molecules are isolated and trapped in the holes. Room-temperature scanning tunneling microscopy (STM) images of h-BN nanomesh with Cu-Pc molecules are shown in Fig. 1 (*12*). The van der Waals diameter of these molecules is 1.5 nm and thus slightly smaller than the 2-nm holes of the nanomesh. The 3.2-nm periodicity of the nanomesh is visible, where at these tunneling conditions the wires map dark (*13*). The brightest objects are identified as single molecules trapped in the holes, although at room temperature they are not completely immobilized, which is reflected in the smearing of the molecular images. An analysis of the center of gravity of 11 molecules in Fig. 1A shows them to be randomly shifted by 0.16 ± 0.1 nm off the center of the corresponding host hole as indicated in the insets.

In order to explore the energy landscape of the nanomesh, we performed photoemission experiments on adsorbed Xe. The bonding of Xe to surfaces resembles in many aspects that of molecules such as Cu-Pc. Thus the Xe electron binding energies and the Xe desorption temperatures provide direct insight into the interplay between the surface electronic dipoles and the bonding caused by polarization. The electrostatic landscape in front of a surface is reflected in the Xe core-level binding energy that aligns to the local vacuum level at the atom core position (*14*–*17*), whereas the Xe desorption temperatures indicate the local bonding strength (*18*).

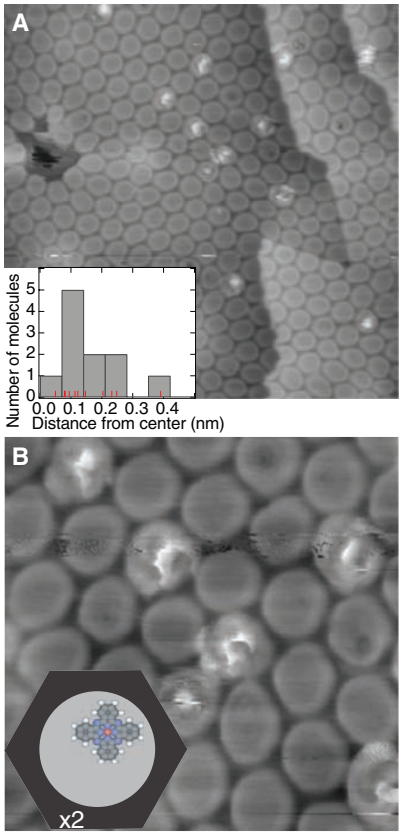

Fig. 1. Room-temperature STM images of a low coverage of Cu-Pc ($C_{32}H_{16}CuN_8$) trapped in the holes of the nanomesh. At the given tunneling conditions, the mesh wires map dark and the holes map bright. Cu-Pc molecules are imaged as bright objects. Current = 30 pA, bias voltage = 1.2 V; images were obtained by horizontal scanning at a rate of 1.8 Hz. (**A**) Overview image (50 by 50 nm). Eleven of 300 nanomesh holes were occupied by molecules. Two monoatomic steps of the Rh substrate and a defect are resolved. The inset shows the distribution of the distances of the molecular center of gravity from the hole center. (**B**) High-resolution image (18 by 18 nm). The inset shows a magnified model of the trapped Cu-Pc molecule.

[1]Physik-Institut, Universität Zürich, Winterthurerstrasse 190, CH-8057 Zürich, Switzerland. [2]Swiss Light Source, Paul Scherrer Institute, CH-5232 Villigen, Switzerland. [3]Institute of Materials Chemistry, Vienna University of Technology, Getreidemarkt 9/165-TC, A-1060 Vienna, Austria.

*Present address: Department of Physics, University of Basel, Klingelbergstrasse 82, CH-4056 Basel, Switzerland. †To whom correspondence should be addressed. E-mail: greber@physik.uzh.ch

Figure 2A displays a series of normal emission spectra obtained during the controlled temperature rise that leads to desorption of a multilayer of Xe on the nanomesh. Four different regimes can be discriminated: the multilayer regime below 63 K; a region between 63 and 72 K [coexistence (C) phase], where two Xe 5p doublets are present; followed by a regime up to 81 K with only one doublet [ring (R) phase]; and above this temperature no Xe features are visible. Energy distribution curves obtained along the dashed lines in Fig. 2A are representative for each of these regions and are plotted in Fig. 2B. The spectrum at 82 K shows the bare nanomesh with the σ_α band at 4.5 eV, which reflects the wires (W), and the σ_β band (at 5.6 eV) associated with the holes (H) (*4*, *7*). The spectrum at 75 K represents the R phase. It shows one Xe $5p_{3/2}$ $5p_{1/2}$ doublet and the nanomesh σ_α (wire) band. Taking into account that the short mean free path of photoelectrons strongly damps the signal from the substrate if it is covered with a single layer of Xe, we assign this doublet (H) to Xe in the holes of the nanomesh (Fig. 2C). At 66 K, in the C phase, two 5p doublets labeled H and W were observed. The doublet W corresponds to Xe on the wires (Fig. 2D), because its disappearance coincides with the appearance of the σ_α (wire) band.

From the van der Waals radius of Xe of 0.22 nm, we estimate the monolayer coverage to be about 54 ± 1 Xe atoms per nanomesh unit cell. If we assume proportionality of Xe coverage and photoemission intensity, this value corresponds to 25 Xe atoms on the wires and 29 Xe atoms in the holes of the nanomesh unit cell. Some Xe in the holes desorbs at higher temperatures and is bound more strongly.

In the *C* phase, the difference in photoemission binding energy between the Xe adsorbed on H and W sites on the substrate is 310 ± 5 meV. We assign these states to regions of different local work functions, where that on the wires is greater than that in the holes. This difference in energy is in good agreement with the theoretical prediction of 0.5 eV (Fig. 3A) (*19*). Extrapolating the Xe $5p_{1/2}$ binding energy to zero coverage, and using the work function as determined from the secondary electron cutoff of 4.15 eV, we obtain a binding

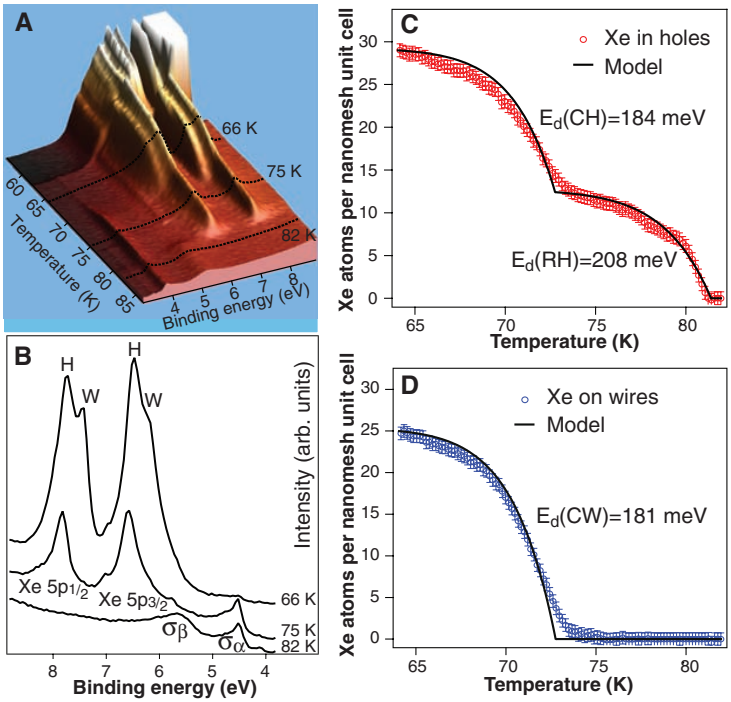

Fig. 2. Temperature dependence of normal emission valence band photoemission spectra from Xe/h-BN/Rh(111). (**A**) Three-dimensionally rendered data set of the desorption of Xe. The dashed lines indicate where the spectra in (B) are derived from. (**B**) Energy distribution curves extracted for three different temperatures (66, 75, and 82 K) as indicated by the dashed lines in (A). (**C**) Spectral weight of the Xe in the holes as a function of temperature. E_d(CH) and E_d(RH) are the two distinct desorption energies from the holes. (**D**) Spectral weight of the Xe on the wires as a function of temperature. E_d(CW) is the desorption energy of Xe from the wires. The solid lines in (C) and (D) are fits obtained from a zero-order desorption model.

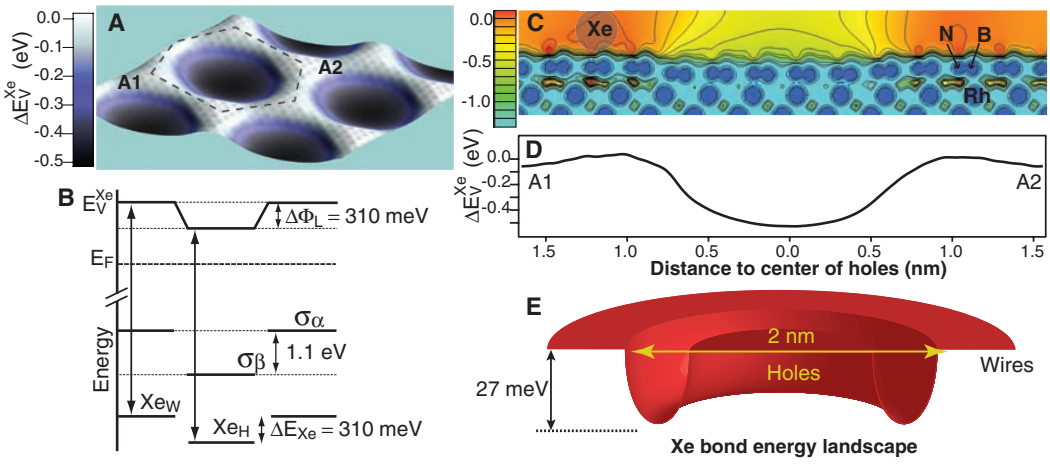

Fig. 3. Energy landscapes of the nanomesh. (**A**) Calculated electrostatic potential 0.38 nm above the nitrogen atoms. The electrostatic potential above the wires is taken as a reference. The potential in the holes attracts negative charge and is 0.5 eV lower. The potential varies because of locally different charge transfer from the h-BN to the substrate and reflects the dipole rings. (**B**) Schematic representation of the observed photoemission line energies from Xe and the h-BN σ bands on the wires (W) σ_α and in the holes (H) σ_β, respectively. The binding energy difference between Xe_W and Xe_H, ΔE_{Xe}, reflects a difference in the electrostatic potential $\Delta\Phi_L$ at different Xe core positions E_V^{Xe}. (**C**) Vertical cut (5.58 by 1.1 nm) across the unit cell containing points A1 and A2 [see (A)]. The color code and the contours reflect the peculiar electrostatic potential energy landscape. The depicted van der Waals contour of the Xe atom is placed at a site on wires where $E_V^{Xe} = = 0$ (**D**) Electrostatic potential along a line connecting A1 and A2, 0.38 nm above the nitrogen atom cores. (**E**) Bond energy landscape for Xe as derived from the thermal desorption data in Fig. 2, C and D. We propose that the strongest bonding sites are related with the dipole rings at the rims of the holes.

energy relative to the vacuum level of 12.0 eV. This value is between those observed for the first and second layer of Xe on metals (*20*) and indicates that the h-BN sheet has a nonmetallic dielectric response similar to that of one layer of Xe (*21*, *22*).

The photoemission binding energies are summarized in Fig. 3B. It rationalizes the peculiar vacuum energy landscape of the nanomesh, where the holes are local low-work-function patches with a diameter of 2 nm. E_V^{Xe} is the electrostatic potential at the Xe atom cores and varies within the nanomesh unit cell. Figure 3A shows the calculated electrostatic potential at the position of the Xe cores, 0.38 nm above the nitrogen atom cores. The potential has a corrugation amplitude of 0.5 eV, which is reflected in the Xe 5p photoemission final state energies. In Fig. 3, C and D, the potential is shown along the two nonequivalent points A1 and A2 in the nanomesh unit cell. The lower potential in the holes is a consequence of stronger hybridization and concomitant charge transfer from the h-BN mesh to the substrate. It causes lateral electric fields, where electrostatic lensing and an influence on the bonding can be expected.

In order to explore the bonding strength, the data in Fig. 2 were analyzed with kinetic desorption models. The Xe bond energy difference is not expected to be as large as the 310 meV for electrons, because Xe atoms are closed-shell and desorb as neutral species. In the following discussion, the temperature dependence of the Xe desorption from the nanomesh is used to confirm the site-dependent bonding and to corroborate the dipole ring hypothesis.

The peak intensities obtained from the fitting of two Gaussians to the peaks labeled H and W in the Xe $5p_{1/2}$ spectrum are shown in Fig. 2, C and D. All Xe on the wires desorbs at lower temperatures, whereas some Xe in the holes remains longer on the surface. If we take the bond energy to be proportional to the maximum desorption temperature, we find that the Xe atoms on the wires are 15% and those in the holes up to 27% more strongly bound than Xe on Xe (multilayer desorption).

Thermal desorption from the holes occurs both in the C phase, where H-Xe and W-Xe coexist (see spectrum at 66 K in Fig. 2B), and in the R phase, without W-Xe. In the C phase, the ratio between H-Xe and W-Xe is almost constant. An Arrhenius analysis shows that the bond energy difference of the desorbing W-Xe and the H-Xe is less than 5 meV. Xe in the R phase is located in the holes and has a higher bond energy. At 73 K, the R phase comprises about 12 Xe atoms per hole, which corresponds to a compact island with a diameter of 1.6 nm, or to a ring with an outer diameter of 2.1 nm. In order to quantitatively access the Xe bond energies, the data were compared to zero-order kinetics. The desorption rates $-dN/dt$ of a given component are

$$-\frac{dN}{dt} = \nu \cdot N^0 \cdot e^{-E_d/kT} \qquad (1)$$

where ν is an attempt frequency in the order of Xe vibration frequencies (2×10^{11} s^{-1}) (*23*) and E_d is the desorption energy. The thermal energy kT is related via the heating rate $\beta = dT/dt$ to the desorption rate. With the corresponding initial coverages, integration of Eq. 1 then leads to $N(T)$.

This model with E_d as a single free parameter fits the observed desorption for all three components quite well. In the C phase, we obtain E_d(CW) = 181 meV and E_d(CH) = 184 meV for the holes and wires, respectively, and in the R phase E_d(RH) = 208 meV. The relative accuracy of these values is better than 1%. The results for the C phase confirm a small energy difference between Xe in the holes and on the wires. The average value is near the bond energy of Xe in the second layer on Ru(0001) (169 meV) (*15*) and confirms that one layer of Xe on Ru(0001) produces a similar bond to Xe as one monolayer of h-BN on Rh(111). On the other hand, the R phase exhibits substantial extra bonding of the Xe.

The question of where inside the hole the atoms of the R phase are located is not directly answered by the desorption kinetics. We see no other physical cause for the extra bonding than the dipole rings, which are located at the rims of the holes. This model is in line with the similar Xe bonding in the C phase for Xe on the wires and some of the Xe in the holes. Also, the size of a Xe_{12} ring exactly fits to the rim of a 2-nm hole, and the tendency of Cu-Pc to sit in the hole, but off center, supports this assignment. Furthermore, the extra bond energy of 24 meV exceeds that of a single Xe-Xe bond (20 meV), which in turn gives an argument for a stabilization of an open structure with low-coordinated atoms, despite the higher coordination within a compact island. Figure 3E shows a schematic drawing of the Xe bond energy landscape on the nanomesh, with extra bonding at the rim of the nanomesh holes, where the electrostatic potential gradient is largest. The polarization-induced increase in bond energy is expected to depend on the size and polarizability of the molecule. The in-plane polarizability of Cu-Pc is more than a factor of 30 greater than that of Xe (*24*), and thus provides an explanation of the room-temperature trapping of large polarizable molecules.

The strong bonding sites are proposed to lie on the rim of the nanomesh holes and are reminiscent of the quantum corrals built atom by atom by Eigler *et al*. (*25*, *26*). Our findings suggest that such seemingly artificial structures may also form or be preformed at once and in huge quantities in a self-assembly process on a suitable template such as the nanomesh. The vacuum energy landscape of the nanomesh, which is imposed by dipole rings, gives a physical basis for such a functionality. This concept should also explain the trapping of larger molecules in periodic arrays on a single-layer dielectric at room temperature. We expect that dipole rings will be found in other nanostructures and that they are a quite general scheme to obtain the immobilization of molecules on surfaces.

References and Notes

1. K. Hermann, B. Gumhalter, K. Wandelt, *Surf. Sci.* **251/252**, 289 (1990).
2. M. Morgenstern, T. Michely, G. Comsa, *Phys. Rev. Lett.* **77**, 703 (1996).
3. L. Nony *et al*., *Nano Lett.* **4**, 2185 (2004).
4. H. Brune, M. Giovannini, K. Bromann, K. Kern, *Nature* **394**, 451 (1998).
5. M. Corso *et al*., *Science* **303**, 217 (2004).
6. S. Berner *et al*., *Angew. Chem. Int. Ed*. **46**, 5115 (2007).
7. A. Goriachko *et al*., *Langmuir* **23**, 2928 (2007).
8. R. Laskowski, P. Blaha, Th. Gallauner, K. Schwarz, *Phys. Rev. Lett.* **98**, 106802 (2007).
9. R. Smoluchowski, *Phys. Rev.* **60**, 661 (1941).
10. K. Xing Lu, W. Hipps, X. D. Wang, U. Mazur, *J. Am. Chem. Soc.* **118**, 7197 (1996).
11. J. Åhlund *et al*., *Surf. Sci.* **601**, 3661 (2007).
12. Details of the experimental studies and theoretical calculations are available as supporting material on *Science* Online.
13. R. Laskowski, P. Blaha, *J. Phys. Cond. Mat*. **20**, 064207 (2008).
14. K. Wandelt, *J. Vac. Sci. Technol. A* **2**, 802 (1984).
15. J. Küppers, K. Wandelt, G. Ertl, *Phys. Rev. Lett.* **43**, 928 (1979).
16. N. D. Lang, A. R. Williams, *Phys. Rev. B* **25**, 2940 (1982).
17. Photoemission final state effects; that is, a site dependence of the photo-hole screening, also have to be considered, although within the same layer they can be treated as a constant offset between the local vacuum-level binding energy and the gas-phase Xe 5p final state.
18. W. Widdra *et al*., *Phys. Rev. B* **57**, 4111 (1998).
19. The theoretical work functions of approximate structures based on the commensurate 1 × 1 model, with BN at face-centered cubic (fcc, top) and hexagonal close-packed fcc sites above Rh are 3.7 and 4.0 eV, respectively. The full nanomesh simulations, however, give an average work function of 3.85 eV, with a difference of 0.5 eV between the hole and wire regions. The theoretical predictions are in good agreement with experiment, although theory does not consider different final-state screening.
20. G. Kaindl, T.-C. Chiang, D. E. Eastman, F. J. Himpsel, *Phys. Rev. Lett.* **45**, 1808 (1980).
21. Considering that the final-state screening decreases with distance from the metal support, we expect a small increase in Xe 5p binding energy (about 50 meV) in climbing the 0.05 nm from the holes to the wires. This effect would lead to a shift to higher Xe-W binding energy, opposite to what is observed here. The photoemission data also show that the σ_α–σ_β splitting of 1.1 eV is not only related to a work function difference, as is expected for a weakly physisorbed system (*22*), but points to differences in the electronic structure of the h-BN wire and hole regions.
22. A. Nagashima, N. Tejima, Y. Gamou, T. Kawai, C. Oshima, *Phys. Rev. Lett.* **75**, 3918 (1995).
23. G. Kerner, O. Stein, Y. Lilach, M. Asscher, *Phys. Rev. B* **71**, 205414 (2005).
24. R. Ramprasad, N. Shi, *Appl. Phys. Lett.* **88**, 222903 (2006).
25. D. M. Eigler, E. K. Schweizer, *Nature* **344**, 524 (1990).
26. E. J. Heller, M. F. Crommie, C. P. Lutz, D. M. Eigler, *Nature* **369**, 464 (1994).

27. The photoemission measurements were performed at the Swiss Light Source, Paul Scherrer Institut, Villigen, Switzerland. We thank the staff at the Surface and Interface Spectroscopy beamline at the Swiss Light Source for assistance. The project was supported by the European Commission under contract NMP4-CT-2004-013817 "NanoMesh" and the Swiss National Science Foundation, contract 200020-116096. Technical support by M. Klöckner, F. Dubi, and C. Hess is gratefully acknowledged.

Supporting Online Material

www.sciencemag.org.cgi/content/full/319/5871/1824/DC1
Materials and Methods
References

14 December 2007; accepted 14 February 2008
10.1126/science.1154179